Howard Hughes Medical Institute

Published as: *Nat Methods*. 2017 October ; 14(10): 987–994.

A general method to fine-tune fluorophores for live-cell and *in vivo* imaging

Jonathan B. Grimm, **Anand K. Muthusamy**, **Yajie Liang**, **Timothy A. Brown**, **William C. Lemon**, **Ronak Patel**, **Rongwen Lu**, **John J. Macklin**, **Phillip J. Keller**, **Na Ji**, and **Luke D. Lavis**[*]

Janelia Research Campus, Howard Hughes Medical Institute, Ashburn, Virginia, USA

Abstract

Pushing the frontier of fluorescence microscopy requires the design of enhanced fluorophores with finely tuned properties. We recently discovered that incorporation of four-membered azetidine rings into classic fluorophore structures elicits substantial increases in brightness and photostability, resulting in the 'Janelia Fluor' (JF) series of dyes. Here, we refine and extend this strategy, showing that incorporation of 3-substituted azetidine groups allows rational tuning of the spectral and chemical properties with unprecedented precision. This strategy yields a palette of new fluorescent and fluorogenic labels with excitation ranging from blue to the far-red with utility in cells, tissue, and animals.

Introduction

Small molecule fluorophores are essential tools for biochemical and biological imaging[1,2]. The development of new labeling strategies[3] and innovative microscopy techniques[4] is driving the need for new fluorophores with specific properties. A particularly useful class of dyes is the rhodamines, first reported in 1887[5], and now used extensively due to the superb brightness and excellent photostability of this fluorophore scaffold[1,2,6]. The photophysical and chemical properties of rhodamines can be modified through chemical substitution[6–14], allowing the creation of fluorescent and fluorogenic labels, indicators, and stains in different colors[7,11–20].

Despite a century of work on this dye class, the design and synthesis of new rhodamines remains severely limited by chemistry. The classic method of rhodamine synthesis—acid

[*]Corresponding author: lavisl@janelia.hhmi.org.

Author Contributions

L.D.L. and J.B.G. conceived the project. J.B.G. contributed organic synthesis and 1-photon spectroscopy measurements. A.K.M. contributed organic synthesis and computational chemistry experiments. Y.J., R.L. and N.J. contributed mouse imaging experiments. T.A.B. contributed cultured cell imaging experiments. W.C.L. and P.J.K. contributed larval explant imaging experiments. R.P. and J.J.M contributed 2-photon spectroscopy measurements. L.D.L. contributed 1-photon spectroscopy measurements and wrote the paper with input from the other authors.

Competing Financial Interests Statement

The authors declare competing interests: J.B.G. and L.D.L. have filed patent applications whose value may be affected by this publication.

catalyzed condensation[2,5,6]—is incompatible with all but the simplest functional groups. To remedy this longstanding problem, our laboratory developed a method to synthesize rhodamine dyes using a Pd-catalyzed cross-coupling strategy starting from simple fluorescein derivatives[21]. This approach facilitated the discovery of a novel class of dyes containing four-membered azetidine rings, which exhibit substantial increases in the quantum yield relative to classic rhodamines containing *N,N*-dimethylamino groups[13]. The flagship member of this new dye class is 'Janelia Fluor 549′ (JF_{549}, **1**, Fig. 1a). The enhanced brightness and photostability of this rhodamine dye has made it an exceptionally useful label for single-molecule experiments in living cells[13,22–25]; the recent development of a photoactivatable derivative has further extended its utility in advanced imaging experiments[26].

An important feature of rhodamine dyes is the ability to tune the spectral and chemical properties using chemistry[13]. JF_{549} (**1**, Fig. 1a, Table 1) absorbs green light ($\lambda_{abs}/\lambda_{em}$ = 549 nm/571 nm, Φ = 0.88), making it an excellent match for light sources centered near 550 nm. Replacing the xanthene oxygen in JF_{549} (**1**) with a quaternary carbon yields carborhodamine Janelia Fluor 608 (JF_{608}, **2**) with an expected[8] 59-nm shift in spectral properties ($\lambda_{abs}/\lambda_{em}$ = 608 nm/631 nm, Φ = 0.67). A larger red-shift can be achieved using the established Si-rhodamine strategy[10,12] to afford Janelia Fluor 646 (JF_{646}, **3**, $\lambda_{abs}/\lambda_{em}$ = 646 nm/664 nm, Φ = 0.54). Finally, a shift to shorter wavelengths can be imposed by replacing one azetidine group in JF_{549} (**1**) with an oxygen atom to yield rhodol[27] Janelia Fluor 519 (JF_{519}, **4**, $\lambda_{abs}/\lambda_{em}$ = 519 nm/546 nm, Φ = 0.85).

In addition to large shifts in λ_{abs} and λ_{em}, these modifications modulate the equilibrium between the colorless, nonfluorescent 'closed' lactone (L) form and the colored, fluorescent, 'open' zwitterionic (Z) form. Rhodamine JF_{549} (**1**, $\varepsilon = 1.01 \times 10^5\ M^{-1}cm^{-1}$), carborhodamine JF_{608} (**2**, $\varepsilon = 9.9 \times 10^4\ M^{-1}cm^{-1}$) and rhodol JF_{519} (**4**, $\varepsilon = 5.9 \times 10^4\ M^{-1}cm^{-1}$) primarily adopt the open, zwitterionic form in water as evidenced by their large extinction coefficients (ε; Table 1). In contrast, JF_{646} (**3**) predominantly adopts the colorless, nonfluorescent, and lipophilic lactone form in aqueous solution ($\varepsilon = 5.0 \times 10^3\ M^{-1}cm^{-1}$). The shifted L–Z equilibrium of JF_{646} and other Si-rhodamines renders these dyes both highly cell permeable, chromogenic, and therefore fluorogenic, where the change in chemical environment upon binding of dye ligands to a variety of biomolecular targets can shift the equilibrium to the fluorescent zwitterionic form[12–14,18].

Despite the flexibility of this fluorophore scaffold and the value in modulating rhodamine properties, the established strategies described above allow only 'coarse' tuning of spectral and chemical attributes: spectral shifts >30 nm and substantial changes in L–Z equilibrium and absorptivity. We sought, and now report, a general method to finely tune the spectral and chemical properties of rhodamine dyes with unprecedented precision. The use of 3-substituted azetidines on the Janelia Fluor 549 (**1**) scaffold allows modulation of λ_{abs}, λ_{em}, and the L–Z equilibrium without affecting fluorescence quantum yield. The shifts in chemical and spectral properties can be justified using physical organic chemistry principles and computational chemistry. The structure–activity relationships determined for rhodamine dyes are generalizable to rhodols, carborhodamines, and Si-rhodamine derivatives, allowing

the rational design of improved fluorescent and fluorogenic labels across the visible spectrum.

Results

Fine-tuning rhodamines: Janelia Fluor 525

We reasoned we could finely tune the physicochemical properties of JF_{549} (**1**) by exploring different substitution patterns on the azetidine ring. Indeed, the azetidinyl-rhodamine system provides an ideal test case for N-substituent effects due to the following: (i) the high-yielding Pd-catalyzed cross-coupling synthesis[21], (ii) the commercial availability of assorted 3-substituted azetidines, (iii) the short, three-bond separation between the substituent and the rhodamine aniline nitrogen, and (iv) the symmetry of the system. We hypothesized that electron withdrawing groups would decrease the λ_{abs} of the fluorophore and also shift the L–Z equilibrium towards the closed, colorless lactone form based on initial computational chemistry experiments (Fig. 1b, **Methods**) and reports of fluoroalkane-substituted rhodamine dyes[19,28].

To test these predictions, we synthesized compounds **5**–**12** (Fig. 1a, Table 1) using our Pd-catalyzed cross-coupling approach[13,21]. We then evaluated the photophysical properties of compounds **5**–**12** in aqueous solution, comparing them to JF_{549} (**1**; Table 1). All of the substituted azetidinyl dyes showed high ε values above 1×10^5 $M^{-1}cm^{-1}$ except for the 3,3-difluoroazetidine compound **12**, which exhibited a slightly lower absorptivity ($\varepsilon = 9.4 \times 10^4$ $M^{-1}cm^{-1}$). Likewise, the quantum yield values of the azetidine dyes **5**–**12** were all >0.80 with the exception of the *N*,*N*-dimethyl-azetidin-3-amine compound **8**, which showed $\Phi =$ 0.57 at pH 7.4. The quantum yield value for **8** is rescued at pH 5.0 ($\Phi = 0.89$; Table 1), suggesting photoinduced electron transfer (PeT) quenching by the unprotonated dimethylamino groups[29].

Although the ε and Φ of the different azetidinyl rhodamine dyes was largely immune to substitution at the 3-position, the λ_{abs} and λ_{em} values were strongly affected by the nature of the substituent (Table 1, Supplementary Fig. 1). Groups with greater electron-withdrawing character elicited larger hypsochromic shifts in λ_{abs}. This effect was additive. For example, the 3-fluoroazetidinyl compound **10** showed a 13-nm blue shift (λ_{abs} = 536 nm) relative to the parent dye **1** and the 3,3-difluoroazetidinyl-rhodamine (**12**) showed a further hypsochromic shift of 11 nm (λ_{abs} = 525 nm). We plotted λ_{abs} against the available Hammett inductive substituent constants (σ_I)[30] for the azetidine substituents in dyes **1**, **5**, and **8**–**12** and observed an excellent correlation (Fig. 1c), suggesting that the inductive effect of the substituents was primarily responsible for the decrease in absorption and emission maxima. The experimental λ_{abs} values also showed excellent agreement with calculated λ_{abs} values (Fig. 1b).

We then analyzed how the azetidine substitutions can tune the lactone–zwitterion (L–Z) equilibrium (Fig. 1d), first examining the absorbance of fluorophores **1**, **5**, and **9**–**12** as a function of dielectric constant using dioxane–water titrations[11,16] (Fig. 1e); compounds **6**–**8** were not examined due to the ionizable substituents on the azetidine ring. Based on these data, we determined the equilibrium constant ($K_{L–Z}$)[31] in 1:1 dioxane:water, which gave the

largest distribution of absorbance measurements (Fig. 1f) and therefore $K_{L–Z}$ values (Fig. 1d, Table 1). We determined these equilibrium values from the maximal extinction coefficients (ε_{max}) measured in acidic alcohol (Table 1, Methods). JF_{549} (**1**) and the 3,3-dimethylazetidinyl-rhodamine **5** showed $K_{L–Z}$ values >3, indicating that these dyes exist primarily in the open form. In contrast, the equilibrium constant of the 3,3-difluoroazetidinyl rhodamine (**12**) was substantially smaller ($K_{L–Z}$ = 0.068), showing that the electron-withdrawing fluorine substituents can shift the equilibrium toward the closed lactone form. The remainder of the dyes exhibited $K_{L–Z}$ values that were intermediate and correlated with σ_I (Fig. 1g). Collectively, these results yield rational and general rules for tuning both λ_{abs} and the L–Z equilibrium using different 3-substituted azetidines without compromising fluorophore brightness.

Rhodamine **12** exhibits λ_{abs} at 525 nm and a high quantum yield (Φ = 0.91), making it a useful label for imaging with blue-green excitation (514–532 nm). Based on the λ_{abs}, we named this fluorophore ‘Janelia Fluor 525′ (JF_{525}) and prepared the JF_{525}–HaloTag[32] ligand (**13**, Fig. 1h), which showed excellent labeling in live cells expressing histone H2B–HaloTag fusions (Fig. 1i). We posited that the JF_{525}–HaloTag ligand (**13**) would show improved cell permeability relative to the parent JF_{549}–HaloTag ligand (**14**, Fig. 1h) based on its higher propensity to adopt the lactone form (Fig. 1d–f, Table 1). We therefore compared the labeling efficiency of **13** or JF_{549}–HaloTag ligand **14** in live cells expressing HaloTag–histone H2B fusions (**Methods**). Compound **13** labeled intracellular proteins faster than JF_{549} ligand **14** (Fig. 1j). These results support the hypothesis that shifting the L–Z equilibrium towards the lactone form can improve cell permeability. We also synthesized the JF_{525}–SNAP-tag ligand **15**, which was useful for intracellular labeling (Supplementary Fig. 2a,b), validating JF_{525} as the first cell-permeable self-labeling tag ligand with an excitation maximum near 532 nm. None of the reported HaloTag or SNAP-tag ligands showed acute cellular toxicity at standard labeling concentrations and incubation times (Supplementary Fig. 2c)

Fine-tuning rhodols: Janelia Fluor 503

Since fluorine is the most electronegative atom, the difluoroazetidine-containing JF_{525} (**12**) represents the tuning limit of the azetidinyl-rhodamines towards the blue region of the spectrum. To access shorter wavelength dyes, we turned to the rhodol Janelia Fluor 519 (**4**, Fig. 1a, Fig. 2a). Based on the tuning rules determined for the rhodamine dyes (Fig. 1a) we surmised that replacement of the single azetidine substituent with a 3,3-difluoroazetidine could elicit a desirable ~15 nm blue-shift to yield a dye with maximal absorption closer to 488 nm. To test this hypothesis, we synthesized the 3,3-difluoroazetidinyl-rhodol **16**, which showed the expected blue-shifted spectra with $\lambda_{abs}/\lambda_{em}$ = 503 nm/529 nm, ε = 8.3×10^4 $M^{-1}cm^{-1}$, and Φ = 0.87 (Fig. 2a, Table 1, Supplementary Fig. 1); we named this compound ‘Janelia Fluor 503′ (JF_{503}).

We then synthesized the JF_{503}–HaloTag ligand (**17**, Fig. 2b), which was an excellent label for histone H2B–HaloTag fusions in live cells (Fig. 2c). We compared this novel label to two other 488 nm-excited HaloTag ligands based on the classic rhodamine 110 ($\lambda_{abs}/\lambda_{em}$ = 497 nm/520 nm; **18**) and the recently described *N*,*N*′-bis(2,2,2-trifluoroethyl)rhodamine (λ_{abs}/

λ_{em} = 501 nm/525 nm; **19**, Supplementary Fig. 2d)[19]. The cell-loading time course for these structurally distinct and relatively polar dyes was similar (Supplementary Fig. 2e) but the JF_{503} ligand showed higher photostability than the other two dyes in live cells (Fig. 2d), consistent with previous reports comparing the photostability of rhodols to rhodamines[27]. JF_{503} could be extended to the SNAP-tag labeling system with JF_{503}–SNAP-tag ligand (**20**; Supplementary Fig. 2f,g).

Fine-tuning carborhodamines: Janelia Fluor 585

In previous work, we extended our Pd-catalyzed cross-coupling approach to carborhodamines[11], resulting in the synthesis of JF_{608} (**2**, Fig. 1a, Fig. 2e, Table 1)[13]. We also discovered that carborhodamines generally exhibit a higher propensity to adopt the colorless lactone form compared to rhodamines ($K_{L–Z}$ for **2** = 0.091). Nevertheless, this shift in the L–Z equilibrium is not sufficient to achieve fluorogenic ligands and its relatively long λ_{abs} value makes JF_{608} suboptimal for multicolor cellular imaging experiments using orange (*e.g.*, 589 nm) and red (*e.g.*, 640 nm) excitation. Based on the rhodamine tuning (Fig. 1a) we expected that incorporation of a 3,3-difluoroazetidine would elicit a blue-shift of approximately 24 nm, bringing the λ_{abs} closer to the desired excitation wavelengths. We were also curious if this modification would create a fluorogenic label since, in the rhodamine series, the 3,3-difluoroazetidine motif decreased the $K_{L–Z}$ by nearly two log units (Fig. 1d). Given the linear relationship between log $K_{L–Z}$ and σ_I (Fig. 1g) we reasoned that this substitution should tune the equilibrium of JF_{608} (**2**, $K_{L–Z}$ = 0.091) closer to the fluorogenic JF_{646} (**3**, $K_{L–Z}$ = 0.0012; Table 1). We note previous efforts to shift the L–Z equilibrium of carborhodamines using direct fluorination produced a HaloTag ligand with modest, nine-fold fluorogenicity, but this modification severely decreased quantum yield[19]. Based on the general trend to higher Φ values upon incorporation of electron-withdrawing substituents in both rhodamines and rhodols (Table 1), we expected that substitution with fluorine atoms on the 3-position of azetidine would increase quantum yield.

To test these predictions, we synthesized the 3,3-difluoroazetidinyl carborhodamine (**21**), which showed the expected blue-shift in spectra ($\lambda_{abs}/\lambda_{em}$ = 585 nm/609 nm) and increase in quantum yield (Φ = 0.78; Fig. 2e, Table 1, Supplementary Fig. 1). Based on these properties the dye was named ‘Janelia Fluor 585′ (JF_{585}). As predicted, JF_{585} (**21**) also exhibited low visible absorption in water ($\varepsilon = 1.5 \times 10^3\ M^{-1}cm^{-1}$) and a $K_{L–Z}$ near zero (Table 1). We then evaluated these carborhodamines as biomolecule labels, preparing JF_{608}–HaloTag ligand (**22**) and JF_{585}–HaloTag ligand (**23**, Fig. 2f)[11,13,21]. We first determined the absorbance of these ligands in the absence and presence of excess HaloTag protein. JF_{608}–HaloTag ligand (**22**) showed only an 11% increase in absorption upon reaction with the HaloTag protein, but JF_{585} ligand **23** showed a substantially higher absorbance increase of 80-fold (Fig. 2g). We then evaluated these dyes in ‘no wash’ cellular imaging experiments. Incubation of JF_{608}–HaloTag ligand (**22**, 250 nM) with cells expressing histone H2B–HaloTag showed excellent nuclear labeling but high background due to the free ligand staining internal membrane structures (Fig. 2h). In contrast, cells that were incubated with 250 nM of JF_{585}–HaloTag ligand **23** and imaged directly showed bright nuclei with low fluorescence background (Fig. 2i). The JF_{585}–SNAP-tag ligand (**24**) also functioned as a cellular label (Supplementary Fig. 2h,i), and the orange JF_{585}–HaloTag ligand (**23**) could be

used in three-color experiments with the green JF_{503}–SNAP-tag ligand (**20**) and our previously described red JF_{646}–Hoechst stain[33] (Supplementary Fig. 2j).

Tuning of Si-rhodamines: Janelia Fluor 635

Having success in applying these tuning rules to rhodol and carborhodamine dyes, we then turned to the Si-rhodamine JF_{646} (**3**, Fig. 1a, Fig. 2j)[13]. We anticipated that addition of a single fluorine atom on each azetidine ring would elicit a ~13 nm hypsochromic shift and further decrease $K_{L–Z}$, yielding a dye with a λ_{abs} near 633 nm and higher degree of fluorogenicity. True to this prediction, the synthesis of the desired fluorinated derivative **25** (Fig. 2j) afforded a dye that showed $\lambda_{abs}/\lambda_{em}$ = 635 nm/652 nm and a slightly higher Φ = 0.56 relative to JF_{646} (**3**). Compound **25** also exhibited an extremely low absorbance in water with an extinction coefficient value of approximately 400 $M^{-1}cm^{-1}$, which gave a $K_{L–Z}$ near zero (Table 1, Supplementary Fig. 1). Based on these data we gave this dye the moniker ‘Janelia Fluor 635′ (JF_{635}).

Analogous to the experiments with JF_{608} and JF_{585}, we synthesized the JF_{635}–HaloTag ligand (**27**) and compared it to the JF_{646} ligand **26** (Fig. 2k). As reported previously[13], ligand **26** shows a 21-fold increase in absorbance upon binding to the HaloTag protein (Fig. 2l). The shifted L–Z equilibrium of JF_{635} causes HaloTag ligand **27** to show exceptionally low background and a 113-fold increase in absorbance upon conjugation (Fig. 2l). Both of these absorbance increases are substantially larger than the previously published SiTMR ligand **28** (Supplementary Fig. 2k), which shows a 6.7-fold increase in absorption upon reaction with the HaloTag protein[12,13]. These *in vitro* results were mirrored in no wash cellular imaging experiments, where we incubated cells expressing histone H2B–HaloTag fusions with 250 nM ligands **26**–**28**. JF_{646} ligand **26** (Fig. 2m) and JF_{635} ligand **27** (Fig. 2n) exhibited substantially lower nonspecific extranuclear fluorescence than the SiTMR compound **28** (Supplementary Fig. 2l) with JF_{635} showing the highest contrast. The SNAP-tag ligand of JF_{635} (**29**) effectively labels SNAP-tag fusions in cells (Supplementary Fig. 2m,n) and the JF_{635}–HaloTag ligand (**27**) could be used in a two-color experiment with JF_{525}–SNAP-tag ligand (**15**; Supplementary Fig. 2o).

Applications in tissue and *in vivo*

The HaloTag ligands of tuned fluorophores Janelia Fluor 585 (**23**) and Janelia Fluor 635 (**27**) are small, cell permeable, and exhibit high fluorogenicity upon reactyion with the HaloTag protein. We were curious if these properties would make them useful for labeling in more complex biological environments such as tissue or whole animals. We first attempted labeling in living brain tissue from *Drosophila* larvae using the JF_{635}–HaloTag ligand (**27**, Fig. 2k) due to its far-red excitation (Fig. 2j, Table 1) and high on:off ratio (Fig. 2l,n). We used a *Drosophila* GAL4 line expressing myristoylated HaloTag protein in ‘Basin’ neurons, which project basin-shaped arbors into the ventral nerve cord (VNC) of the larval fly[34]. Explants from *Drosophila* third instar larvae were dissected, incubated briefly with **27** (1 μM, 10 min), and imaged using the SiMView light-sheet microscope[35]. As shown in the projection of the SiMView 3D-reconstruction, the JF_{635} label exhibited consistent labeling throughout the living tissue and low nonspecific background staining (Fig. 3a,b, Supplementary Fig. 3a–c), demonstrating its utility beyond simple cell culture.

We next evaluated the JF dyes in the brains of living mice. The JF_{585}–HaloTag ligand **23** was chosen based on its high fluorogenicity (Fig. 2g,i) and superior 2-photon fluorescence at 1100 nm excitation (Fig. 3c), which is sufficiently separated from GFP-based indicators such as GCaMP6 (2-photon λ_{ex} = 940 nm)[36] to allow multicolor imaging. Cytosolic HaloTag protein was co-expressed in layer 4 or layer 5 visual cortex (V1) neurons with GCaMP6s via viral transduction and the mice were fitted with a chronic cranial window (**Methods**). Injection of 100 nmol of HaloTag ligand **23** into the tail vein (intravenous, IV) showed the JF_{585} ligand was blood–brain barrier-permeable and gave measureable labeling in the brain within 5 minutes, peaking around 6 hours and lasting for nearly two weeks as measured by epifluorescence (Fig. 3d, Supplementary Fig. 3d). Subsequent intraperitoneal injection (IP) into the same set of mice also showed effective delivery to the brain, although with different pharmacokinetics in the early time points (<7 days; Fig. 3d). Under 2-photon imaging, we observed that the GCaMP6s and JF_{585} signals co-localized (Fig. 3e, Supplementary Fig. 3e, Supplementary Video 1), and the labeling showed no significant effect on spontaneous neuronal activity (Fig. 3f,g), establishing the utility of this fluorophore *in vivo*.

Discussion

Despite the broad utility of rhodamines, the extant methods to modulate the physicochemical properties of this dye class are relatively coarse and empirical. Here, we describe a new method that allows rational fine-tuning of fluorophore properties for specific biological applications. We first determined the tuning rules in the rhodamine system by synthesizing a panel of rhodamine variants using the bright and photostable JF_{549} scaffold (Fig. 1a). This resulted in the development of JF_{525} (**12**) and its derivatives **13** and **15**, which constitute the first ligands for self-labeling tags with absorption maxima near 532 nm. The tuning rules discovered are generalizable to other fluorophore classes—rhodols, carborhodamines, and Si-rhodamines—allowing the rational design of finely-tuned fluorophores such as JF_{503} (**16**, Fig. 2a), JF_{585} (**21**, Fig. 2e), and JF_{635} (**25**, Fig. 2j). Together with JF_{549} (**1**) and JF_{646} (**3**, Fig. 1a)[13], we have now described six dyes that span the visible region of the spectrum and match common excitation wavelengths for fluorescence microscopy. These bright fluorophores can be used immediately for structured illumination (SIM) and stimulated emission depletion (STED) imaging and could be converted to photoactivatable derivatives[26] for single-molecule localization microscopy (SMLM) experiments. Our general rules should allow fine-tuning of a variety of fluorescent reagents including classic fluorophores[13], emerging red-shifted rhodamine variants[37], and fluorogenic ligands[12,14,18,19,33] to further extend the range of bright fluorophores useful for fluorescence microscopy. Importantly, the new HaloTag ligands derived from JF_{585} and JF_{635} show a high degree of chromogenicity and fluorogenicity (Fig. 2g,i,l,n), a critical parameter in advanced imaging experiments[38]. Of particular interest is the ability to deliver these dyes to neural tissue in explants (Fig. 3a,b) or whole animals (Fig. 3d–g), which could allow the imaging of deeper structures in the brain or the *in vivo* assembly of semisynthetic indicators for monitoring cellular activity[3].

Although we focused on the fluorine-substituted azetidines in this paper, the other substitutions (Fig. 1a) could be exploited to prepare fluorophores for specific applications. For example, the carboxy groups in compounds **6** and **7** could serve as attachment sites for a

variety of chemical modifiers to improve solubility[7], quench unwanted triplet states[39], or allow the molecule to serve as a multivalent fluorescent cross-linker. The modest pH sensitivity and presence of the basic amine in compound **8** could allow it to function as a pH sensor or stain for lysosomes. The methoxy group on compound **9** could be elaborated to a polyethylene glycol (PEG) or other solubilizing group. Finally, the cyano group in compound **11** could be used in multimodal imaging regimes where both fluorescence and Raman[40] modalities are used for imaging. In all, this general method to rationally tune photophysical and chemical properties against a backdrop of high quantum yield will allow the precise design of many new fluorophores for specific, sophisticated biological imaging experiments in increasingly complex systems.

Online Methods

Chemical synthesis

Methods for chemical synthesis and full characterization of all novel compounds can be found in the Supplementary Note.

UV–vis and fluorescence spectroscopy

Fluorescent and fluorogenic molecules for spectroscopy were prepared as stock solutions in DMSO and diluted such that the DMSO concentration did not exceed 1% v/v. Spectroscopy was performed using 1-cm path length, 3.5-mL quartz cuvettes or 1-cm path length, 1.0-mL quartz microcuvettes from Starna Cells. All measurements were taken at ambient temperature (22 ± 2 °C). Absorption spectra were recorded on a Cary Model 100 spectrometer (Agilent). Fluorescence spectra were recorded on a Cary Eclipse fluorometer (Varian). Maximum absorption wavelength (λ_{abs}), extinction coefficient (ε), and maximum emission wavelength (λ_{em}) were taken in 10 mM HEPES, pH 7.3 buffer unless otherwise noted; reported values for ε are averages (n = 3). Normalized spectra are shown for clarity.

Determination K_{L-Z} and ε_{max}

To determine K_{L-Z} we first performed dioxane–H_2O titrations in spectral grade dioxane (Aldrich) and milliQ H_2O (Fig. 1e). The solvent mixtures contained 0.01% v/v triethylamine to ensure the rhodamine dyes were in the zwitterionic form. The absorbance values at λ_{abs} were measured on 5 μM samples (n = 4) using a quartz 96-well microplate (Hellma) and a FlexStation3 microplate reader (Molecular Devices). Values of dielectric constant (ε_r) were as previously reported[41]. We then calculated K_{L-Z} using the following equation[31]: $K_{L-Z} = (\varepsilon_{dw}/\varepsilon_{max})/(1 - \varepsilon_{dw}/\varepsilon_{max})$. ε_{dw} is the extinction coefficient of the dyes in a 1:1 v/v dioxane:water solvent mixture (Fig. 1f); this dioxane–water mixture was chosen to give the maximum spread of K_{L-Z} values (Fig. 1e). ε_{max} is the maximal extinction coefficients measured in different solvent mixtures depending on dye type: 0.1% v/v trifluoroacetic acid (TFA) in 2,2,2-trifluoroethanol (TFE) for the rhodamines (**1**, **5**–**12**) and carborhodamines (**2**, **21**); 0.1% v/v TFA in ethanol for the Si-rhodamines (**3**, **25**); 0.01% v/v Et_3N in TFE for the rhodols (**4**, **16**).

Quantum yield determination

All reported absolute fluorescence quantum yield values (Φ) were measured in our laboratory under identical conditions using a Quantaurus-QY spectrometer (model C11374, Hamamatsu). This instrument uses an integrating sphere to determine photons absorbed and emitted by a sample. Measurements were carried out using dilute samples ($A < 0.1$) and self-absorption corrections[42] were performed using the instrument software. Reported values are averages (n = 3). The quantum yield for compound **8** at pH 5.0 was taken in 10 mM sodium citrate buffer containing 150 mM NaCl.

Computational chemistry

Computational experiments were performed using Gaussian 09.[43] DFT and TD-DFT methods were used to calculate the spectral properties of the azetidinyl rhodamine compounds (Fig. 1b). Calculations were performed at the B3LYP/6-31+G(d,p)/IEFPCM and TD-B3LYP/6-31+G(d,p)/IEFPCM theory levels for the ground states and excited states respectively. Frequency calculations confirmed that an energy minimum was found in geometry optimizations. Linear response solvation with the IEFPCM model was sufficient to study the excited state energies. Evaluations of TD-DFT theory have discussed the overestimation of excitation energies[44,45], and previous studies of rhodamine excited states have reported using ~0.4 eV correction to account for this overestimation[46,47]. We applied a consistent –0.4 eV correction to the calculated excited state energies, which gave good agreement with spectroscopy experiments (Fig. 1b).

Measurement of increase in absorbance of HaloTag ligands 22, 23, 26–28 upon attachment with HaloTag protein

HaloTag protein used as a 100 μM solution in 75 mM NaCl, 50 mM TRIS·HCl, pH 7.4 with 50% v/v glycerol (TBS–glycerol). Absorbance measurements were performed in 1 mL quartz cuvettes. HaloTag ligands **22**, **23**, **26**–**28** (5 μM) were dissolved in 10 mM HEPES, pH 7.3 containing 0.1 mg·mL^{-1} CHAPS. An aliquot of HaloTag protein (1.5 equiv) or an equivalent volume of TBS–glycerol blank was added and the resulting mixture was incubated until consistent absorbance signal was observed (~60 min). Absorbance scans are averages (n = 2).

Multiphoton spectroscopy

HaloTag ligands **13**, **14**, **17**, **23**, **26**, and **27** (5 μM) were incubated with excess purified HaloTag protein (1.5 equiv) in 10 mM HEPES, pH 7.3 containing 0.1 mg·mL^{-1} CHAPS as above and incubated for 24 h at 4 °C. These solutions were then diluted to 1 μM in 10 mM HEPES buffer, pH 7.3 and the two-photon excitation spectra were measured as previously described[48,49]. Briefly, measurements were taken on an inverted microscope (IX81, Olympus) equipped with a 60×, 1.2NA water objective (Olympus). Dye–protein samples were excited with pulses from an 80 MHz Ti-Sapphire laser (Chameleon Ultra II, Coherent) for 710–1080 nm and with an OPO (Chameleon Compact OPO, Coherent) for 1000–1300 nm. Fluorescence collected by the objective was passed through a dichroic filter (675DCSXR, Omega) and a short pass filter (720SP, Semrock) and detected by a fiber-coupled Avalanche Photodiode (SPCM_AQRH-14, Perkin Elmer). For reference, a two-

photon excitation spectrum was also obtained for the red fluorescent protein mCherry (1 μM), in the same HEPES buffer. All excitation spectra are corrected for the wavelength-dependent transmission of the dichroic and band-pass filters, and quantum efficiency of the detector.

General cell culture and fluorescence microscopy

COS7 and U2OS cells (ATCC) were cultured in Dulbecco's modified Eagle medium (DMEM, phenol red-free; Life Technologies) supplemented with 10% (v/v) fetal bovine serum (Life Technologies), 1 mM GlutaMAX (Life Technologies) and maintained at 37 °C in a humidified 5% (v/v) CO_2 environment. The COS7 cells have integrated a histone H2B–HaloTag expressing plasmid via the piggyback transposase (*i.e.*, 'H2B–Halo' cells), and the U2OS cells have integrated a Sec61β–HaloTag expressing plasmid via the piggyback transposase. Both cells were kept under the selection of 500 μg/mL Geneticin (Life Technologies). Cell lines undergoes regular mycoplasma testing by the Janelia Cell Culture Facility. Cells were imaged on confocal microscopes in the Janelia Imaging Facility (Zeiss LSM 710, W Plan APO 20×/1.8 D -or- Zeiss LSM 880, C-APO 40×/1.2 W Corr FCS M27) using the indicated filter sets.

Comparison of JF_{549} and JF_{525}

For the dye loading comparison (Fig 1j), H2B-Halo COS7 cells were stained for varying amounts of time with 100 nM of either JF_{525}–HaloTag ligand **13** or JF_{549}–HaloTag ligand **14**. The dye was washed from the cells and subsequently labeled with JF_{646}–HaloTag ligand **26** at 1 μM for 30 min. Fluorescence of JF_{646}–HaloTag ligand was quantified from the nuclear signals in summed confocal image stacks collected with 633 nm Ex/638–759 nm Em and analysed using Fiji.[50] The integrated density of the nuclear signal was corrected by subtracting the integrated density of adjacent background regions. Labeling is expressed as the percent of the JF_{646}–HaloTag fluorescence displaced by the JF_{525}– and JF_{549}–HaloTag ligands. The nuclear staining of these cells by the JF_{525}–HaloTag ligand (Fig. 1i) is displayed as a maximum intensity projection of confocal image stacks, 514 nm Ex/530–657 Em.

Comparison of JF_{503} and other 488 nm-excited dyes

H2B–Halo COS7 cells were labeled with 200 nM of JF_{503}–HaloTag ligand **17**, HaloTag® R110Direct™ ligand (**18**, Promega), or HaloTag ligand **19**[28], over a time course of 0–2 h. Cells were washed 2× with PBS and fixed with 4% w/v paraformaldehyde in 0.1 M phosphate for 30 min, followed by two more washes with PBS. Cells were imaged using confocal microscopy with 488 nm Ex/515–565 nm Em. The nuclear staining of these cells by the JF_{503}–HaloTag ligand (**17**; Fig. 2c) is displayed as a maximum intensity projection of confocal image stacks. Corrected nuclear fluorescence was calculated as above to determine the cell loading profile (Supplementary Fig. 2e). To test the relative bleaching rates of these three dyes under imaging conditions (Fig. 2d), cells were stained and fixed as previously described for 2 h and then bleached with 488 nm at twice the typical power and imaged after each of 70 cycles. Bleached fluorescence data are normalized to the initial fluorescence levels.

Comparison of HaloTag ligands 22, 23, and 26–28 in cells

H2B–Halo COS7 cells were labeled with 250 nM of JF_{608}–HaloTag ligand (**22**), JF_{585}–HaloTag ligand (**23**), JF_{646}-HaloTag ligand (**26**), JF_{635}-HaloTag ligand (**27**), or SiTMR–HaloTag ligand (**28**; Supplementary Fig. 2k) and imaged by confocal microscopy using 594 nm Ex/599–734 nm Em (JF_{608} and JF_{585}) or 633 nm Ex/638–759 nm Em (JF_{646} JF_{635}, or SiTMR). All five samples were imaged via confocal microscopy without washing out the dyes. Signal to noise ratios were determined using the mean fluorescence of the nuclei relative to a region adjacent to each nuclei using Fiji[50] (n = 152–275 areas as noted; Fig. 2h,i,m,n, Supplementary Fig. 2l).

Staining with SNAP-tag ligands

COS7 cells were transfected with histone H2B–pSNAP-tag (New England Biolabs) and stable integration of this plasmid was selected for using 600 μg/mL Geneticin® (Life Technologies). This cell line expresses the histone H2B protein fused to the 26m version of the SNAP-tag protein. Cells were stained with four different dyes as follows; JF_{503}–SNAP-tag ligand (**20**, 2 μM for 90 min), JF_{525}–SNAP-tag ligand (**15**, 3 μM for 30 min), JF_{585}–SNAP-tag ligand (**24**, 2 μM for 3 hr with 0.2% w/v Pluronic F-127), JF_{635}–SNAP-tag ligand (**29**, 2 μM for 2 h with 0.2% w/v Pluronic F-127). After staining, cells were washed three times with complete media, followed by a 20-min incubation in a 37 °C, 5% CO_2, humidified incubator. The media was replaced again immediately prior to imaging.

Multiplexed imaging using HaloTag and SNAP-tag

U2OS cells expressing Sec61β–HaloTag fusion were transfected with either histone H2B–SNAP-tag piggybac orTOMM20–pSNAPf plasmids using Lipofectamine 2000 (ThermoFisher). Sec61β encodes an endoplasmic reticulum membrane protein translocator protein, and TOMM20 encodes an outer mitochondrial membrane protein as part of a protein translocase complex. Live cells were simultaneously stained with combinations of JF_{503}–SNAP-tag ligand (**20**, 1 μM) and JF_{585}–HaloTag ligand (**23**, 100 nM; Supplementary Fig. 2j) or JF_{525}–SNAP-tag ligand (**15**, 1 μM) and JF_{635}–HaloTag ligand (**27**, 100 nM, Supplementary Fig. 2o) for 60 min. Cells were fixed with 4% paraformaldehyde (20 min), and subsequently stained with JF_{646}–Hoechst[33] (5 μM, 30 min), as indicated, prior to imaging.

Cell viability assays

The effects of various Janelia Fluor ligand compounds on cell viability were tested using the tetrazolium dye 3-(4,5-dimethylthiazol-2-yl)-2,5-diphenyltetrazolium bromide (MTT, Supplementary Fig. 2c). This colorimetric cell viability assay relies on NAD(P)H-dependent oxidoreductase enzymes that reduce the dye to an insoluble and highly absorbing formazan[51]. COS7 cells were plated at 1.5×10^4 cells per well of a 96-well plate 24 h prior to the assay. Dyes were applied to cells at different concentrations to span standard labeling conditions in live cells (n = 3). HaloTag ligands **13**, **14**, **17**, **23**, **26**, and **27** were applied for 1 hour and SNAP-tag ligands **15**, **20**, **24**, and **29** were applied for 3 hours prior to addition of MTT to reflect typical maximum staining times for these dyes.

Staining of *Drosophila* larvae

The central nervous system of third instar *Drosophila melanogaster* larvae were dissected in physiological saline. For the JF_{635}–HaloTag ligand staining (Fig. 3a,b, Supplementary Fig. 3a,c), we used larva expressing a previously described[52] HaloTag containing a myristoylation sequence in the 'Basin' neurons under control of the enhancer fragment R72F11.[34] The isolated nervous system was incubated in physiological saline containing 1 μM JF_{635}–HaloTag ligand (**27**) for 10 min at room temperature. For the pan-neuronal comparison (Supplementary Fig. 3b), this animal expressed GCaMP6s via the Gal4/UAS system using a 57C10-Gal4 driver line. The specimens were then embedded in agarose and imaged with the SiMView light-sheet microscope.[35] The VNC zoomed images for direct comparison (Supplementary Fig. 3a,b) show the raw image data after fusion and deconvolution, whereas the full image of JF_{635}–HaloTag ligand labeling (Fig. 3a,b, Supplementary Fig. 3c) additionally uses filtering and gamma correction to show neuronal morphologies more clearly.

General information for mouse *in vivo* experiments

Male mice, 3–8 months old, were used for viral infection, dye injection, and *in vivo* imaging of neurons in the visual cortex (V1): The Scnn1a-Tg3-Cre (Jax no. 009613) line was used for imaging in layer 4 cortical neurons (L4); and Rbp4-Cre mice (MMRRC no. 031125-UCD) were used for imaging in layer 4 cortical neurons (L5) neurons. All experimental protocols were conducted according to the National Institutes of Health guidelines for animal research and were approved by the Institutional Animal Care and Use Committee at the Janelia Research Campus, HHMI.

Cranial window implant and virus injection

A craniotomy was carried out at the same time as the virus injection to provide optical access for *in vivo* imaging experiments. Mice were anesthetized with isoflurane (1–2% v/v in O_2) and given the analgesic buprenorphine (SC, 0.3 mg/kg). Using aseptic technique, a 3.5 mm-diameter craniotomy was made over the left V1 region of the brain of anaesthetized mouse (center: 3.4 mm posterior to Bregma; 2.7 mm lateral from midline). The dura was left intact. HaloTag and GCaMP6s was cotranduced using the viral vector: AAV2/1.synapsin.FLEX.GCaMP6s.P2A.HaloTag.WPRE (~5×10^{12} infectious units per ml, 30 nl per site). The virus was injected using a glass pipette beveled at 45° with a 15–20-μm opening and back-filled with mineral oil. A fitted plunger controlled by a hydraulic manipulator (Narashige, MO10) was inserted into the pipette and used to load and inject the solution into 6 sites of left V1 (3.4–4.4 mm posterior to Bregma; 2.2–2.8 mm lateral from midline; ~0.5 mm distance between each injection site, 0.5 mm below pia). A cranial window made of a single glass coverslip (Fisher Scientific no. 1.5) was embedded in the craniotomy and sealed in place with dental acrylic. A titanium head-post was attached to the skull with cyanoacrylate glue and dental acrylic.

Dye administration *in vivo*

JF_{585}–HaloTag ligand (**23**) was administered to mice 3–4 weeks after the cranial window installation and viral injection. Dye solution was prepared by first dissolving 100 nmol (76

μg) of **23** in 20 μL DMSO. After vortexing, 20 μL of a Pluronic F-127 solution (20% w/w in DMSO) was added and this stock solution was diluted into 100 μL or 200 μL sterile saline for IV (tail vein) or IP injection, respectively.

In vivo wide-field imaging and analysis

Mice were head-fixed and awake during the imaging period and were therefor habituated to experimental handling and head fixation starting 1-week post-surgery. During each habituation session, mice were head-fixed onto the sample stage with body restrained under a half-cylindrical cover. The habituation procedure was repeated 3–4 times for each animal for a duration of 15–60 minutes. For *in vivo* wide-field imaging, an external fluorescence light source (Leica EL6000, Leica) was used for excitation of GCaMP6s (green channel) and JF_{585}–HaloTag ligand (red channel). Images were acquired via Leica Application Suite 4.5 (Leica). Wide-field images in green (1 second exposure) and red (4 second exposure) channels were acquired at multiple time intervals over two weeks under the same imaging conditions and the images were aligned with the Stackreg plugin in ImageJ. The mean values in the same area of red and green channels were plotted to track the labeling kinetics and turnover of JF_{585}–HaloTag *in vivo*.

In vivo two-photon imaging and analysis

For *in vivo* two-photon imaging, GCaMP6s and JF_{585}–HaloTag were excited at 940 nm and 1100 nm, respectively, using a femtosecond laser source (InSight DeepSee, Spectra-Physics), and imaged using an Olympus 25× 1.05 NA objective and a homebuilt two-photon microscope[53]. Images were acquired from 200 to 550 μm below the pia with post-objective power ranging between 20 and 60 mW. No photobleaching or photodamage of tissue was observed. Typical imaging settings were composed of 256 × 256 pixels, with 1.2 μm per pixel, and a ~3 Hz frame rate. The time-lapse calcium images of spontaneous neuronal activity in awake, head fixed mice were recorded and analyzed with custom programs written in MATLAB (Mathworks). Lateral motion present in head-fixed awake mice was corrected using a cross-correlation-based registration algorithm[54], where cross-correlation was calculated to determine frame shift in x and y directions. Cortical neurons were outlined by hand as regions of interest (ROIs). The fluorescence time course of each ROI was used to calculate its calcium transient as $\Delta F/F\ (\%) = (F-F_0)/F_0 \times 100$, with the baseline fluorescence F_0 being the mode of the fluorescence intensity histogram of this ROI. For the Pearson correlation coefficient calculation, the JF_{585} (red channel) and GCaMP6s (green channel) fluorescence signals in each ROI were averages from 1000 imaging frames (3 Hz).

Statistics

For spectroscopy measurements (Fig. 1e,f, Fig. 2g,l, Table 1, and Supplementary Fig. 1) reported n values for absorption spectra, extinction coefficient (ε) and quantum yield (Φ) represent measurements of different samples prepared from the same dye DMSO stock solution. For the cell loading experiment (Fig. 1j) the following reported n values represent the number of intensity values measured from three fields of view for the time points at 30 s, 1 min, 2 min, 3 min, and 4 minutes, respectively: JF_{525}–HaloTag ligand **13**: n= 112, 120, 130, 114, 128; JF_{549}– HaloTag ligand **14**: n = 135, 129, 135, 158, 161. For the reference

stain using JF_{646}–HaloTag ligand n = 248. For cellular toxicity (Supplementary Fig. 2c) assays, reported n values represent different cell culture samples in separate microplate wells. For the contrast measurements (Fig. 2h,i,m,n, Supplementary Fig. 2l) reported n values represent intensity values measured from three fields of view for each dye type. For the IV and IP experiments (Fig. 3d), reported n = 3 values represent different fields of view taken via wide-field imaging. The one-way ANOVA analysis of spontaneous neuronal activity before and after dye administration (Fig. 3g) gave $F(3, 236) = 0.1204$.

Data availability

The data that support the findings of this study are provided in the Source Data files or available from the corresponding author upon request.

Supplementary Material

Refer to Web version on PubMed Central for supplementary material.

Acknowledgments

We thank A. Berro and E. Schreiter (Janelia) for purified HaloTag protein, and H. Choi (Janelia) for the Sec61β–HaloTag plasmid, contributive discussions, and a critical reading of the manuscript. This work was supported by the Howard Hughes Medical Institute.

References

1. Lavis LD, Raines RT. Bright ideas for chemical biology. ACS Chem Biol. 2008; 3:142–155. [PubMed: 18355003]
2. Lavis LD, Raines RT. Bright building blocks for chemical biology. ACS Chem Biol. 2014; 9:855–866. [PubMed: 24579725]
3. Xue L, Karpenko IA, Hiblot J, Johnsson K. Imaging and manipulating proteins in live cells through covalent labeling. Nat Chem Biol. 2015; 11:917–923. [PubMed: 26575238]
4. Liu Z, Lavis LD, Betzig E. Imaging live-cell dynamics and structure at the single-molecule level. Mol Cell. 2015; 58:644–659. [PubMed: 26000849]
5. Ceresole, M. Verfahren zur Darstellung von Farbstoffen aus der Gruppe des Meta-amidophenolphtaleïns. Germany Patent. 44002. 1887.
6. Beija M, Afonso CAM, Martinho JMG. Synthesis and applications of rhodamine derivatives as fluorescent probes. Chem Soc Rev. 2009; 38:2410–2433. [PubMed: 19623358]
7. Panchuk-Voloshina N, et al. Alexa Dyes, a series of new fluorescent dyes that yield exceptionally bright, photostable conjugates. J Histochem Cytochem. 1999; 47:1179–1188. [PubMed: 10449539]
8. Arden-Jacob J, Frantzeskos J, Kemnitzer NU, Zilles A, Drexhage KH. New fluorescent markers for the red region. Spectrochim Acta, Part A. 2001; 57:2271–2283.
9. Liu JX, et al. Rational design and synthesis of a novel class of highly fluorescent rhodamine dyes that have strong absorption at long wavelengths. Tetrahedron Lett. 2003; 44:4355–4359.
10. Koide Y, Urano Y, Hanaoka K, Terai T, Nagano T. Evolution of Group 14 rhodamines as platforms for near-infrared fluorescence probes utilizing photoinduced electron transfer. ACS Chem Biol. 2011; 6:600–608. [PubMed: 21375253]
11. Grimm JB, et al. Carbofluoresceins and carborhodamines as scaffolds for high-contrast fluorogenic probes. ACS Chem Biol. 2013; 8:1303–1310. [PubMed: 23557713]
12. Lukinavičius G, et al. A near-infrared fluorophore for live-cell super-resolution microscopy of cellular proteins. Nature Chem. 2013; 5:132–139. [PubMed: 23344448]
13. Grimm JB, et al. A general method to improve fluorophores for live-cell and single-molecule microscopy. Nat Methods. 2015; 12:244–250. [PubMed: 25599551]

14. Lukinavicius G, et al. Fluorogenic probes for multicolor imaging in living cells. J Am Chem Soc. 2016; 138:9365–9368. [PubMed: 27420907]
15. Lavis LD, Chao TY, Raines RT. Fluorogenic label for biomolecular imaging. ACS Chem Biol. 2006; 1:252–260. [PubMed: 17163679]
16. Watkins RW, Lavis LD, Kung VM, Los GV, Raines RT. Fluorogenic affinity label for the facile, rapid imaging of proteins in live cells. Org Biomol Chem. 2009; 7:3969–3975. [PubMed: 19763299]
17. Wysocki LM, et al. Facile and general synthesis of photoactivatable xanthene dyes. Angew Chem, Int Ed. 2011; 50:11206–11209.
18. Lukinavicius G, et al. Fluorogenic probes for live-cell imaging of the cytoskeleton. Nat Methods. 2014; 11:731–733. [PubMed: 24859753]
19. Butkevich AN, et al. Fluorescent rhodamines and fluorogenic carbopyronines for super-resolution STED microscopy in living cells. Angew Chem Int Ed. 2016; 55:3290–3294.
20. Grimm JB, et al. Synthesis of a far-red photoactivatable Si-rhodamine for super resolution microscopy. Angew Chem Int Ed. 2016; 55:1723–1727.
21. Grimm JB, Lavis LD. Synthesis of rhodamines from fluoresceins using Pd-catalyzed C–N cross-coupling. Org Lett. 2011; 13:6354–6357. [PubMed: 22091952]
22. Liu Z, et al. 3D imaging of Sox2 enhancer clusters in embryonic stem cells. Elife. 2014; 3:e04236. [PubMed: 25537195]
23. Knight SC, et al. Dynamics of CRISPR-Cas9 genome interrogation in living cells. Science. 2015; 350:823–826. [PubMed: 26564855]
24. Swinstead EE, et al. Steroid receptors reprogram FoxA1 occupancy through dynamic chromatin transitions. Cell. 2016; 165:593–605. [PubMed: 27062924]
25. Bisson-Filho AW, et al. Treadmilling by FtsZ filaments drives peptidoglycan synthesis and bacterial cell division. Science. 2017; 355:739–743. [PubMed: 28209898]
26. Grimm JB, et al. Bright photoactivatable fluorophores for single-molecule imaging. Nat Methods. 2016; 13:985–988. [PubMed: 27776112]
27. Whitaker JE, et al. Fluorescent rhodol derivatives: Versatile, photostable labels and tracers. Anal Biochem. 1992; 207:267–279. [PubMed: 1481981]
28. Mitronova GY, et al. New fluorinated rhodamines for optical microscopy and nanoscopy. Chem Eur J. 2010; 16:4477–4488. [PubMed: 20309973]
29. Asanuma D, et al. Acidic-pH-activatable fluorescence probes for visualizing exocytosis dynamics. Angew Chem Int Ed. 2014; 126:6199–6203.
30. Hansch C, Leo A, Taft RW. A survey of Hammett substituent constants and resonance and field parameters. Chem Rev. 1991; 91:165–195.
31. Hinckley DA, Seybold PG. A spectroscopic/thermodynamic study of the rhodamine B lactone–zwitterion equilibrium. Spectrochim Acta, Part A. 1988; 44:1053–1059.
32. Los GV, et al. HaloTag: A novel protein labeling technology for cell imaging and protein analysis. ACS Chem Biol. 2008; 3:373–382. [PubMed: 18533659]
33. Legant WR, et al. High-density three-dimensional localization microscopy across large volumes. Nat Methods. 2016; 13:359–365. [PubMed: 26950745]
34. Ohyama T, et al. A multilevel multimodal circuit enhances action selection in Drosophila. Nature. 2015; 520:633–639. [PubMed: 25896325]
35. Lemon WC, et al. Whole-central nervous system functional imaging in larval Drosophila. Nat Commun. 2015; 6:7924. [PubMed: 26263051]
36. Chen TW, et al. Ultrasensitive fluorescent proteins for imaging neuronal activity. Nature. 2013; 499:295–300. [PubMed: 23868258]
37. Zhou X, Lai R, Beck JR, Li H, Stains CI. Nebraska Red: A phosphinate-based near-infrared fluorophore scaffold for chemical biology applications. Chem Commun. 2016; 52:12290–12293.
38. Bruchez MP. Dark dyes–bright complexes: Fluorogenic protein labeling. Curr Opin Chem Biol. 2015; 27:18–23. [PubMed: 26056741]
39. Altman RB, et al. Cyanine fluorophore derivatives with enhanced photostability. Nat Methods. 2012; 9:68–71.

40. Palonpon AF, Sodeoka M, Fujita K. Molecular imaging of live cells by Raman microscopy. Curr Op Chem Biol. 2013; 17:708–715.

Methods-Only References

41. Critchfield FE, Gibson JA Jr, Hall JL. Dielectric constant for the dioxane–water system from 20 to 35°. J Am Chem Soc. 1953; 75:1991–1992.

42. Suzuki K, et al. Reevaluation of absolute luminescence quantum yields of standard solutions using a spectrometer with an integrating sphere and a back-thinned CCD detector. Phys Chem Chem Phys. 2009; 11:9850–9860. [PubMed: 19851565]

43. Frisch, MJ., et al. Gaussian 09, revision D. 01. Gaussian, Inc; Wallingford CT: 2009.

44. Dreuw A, Weisman JL, Head-Gordon M. Long-range charge-transfer excited states in time-dependent density functional theory require non-local exchange. J Chem Phys. 2003; 119:2943–2946.

45. Jacquemin D, et al. Assessment of the efficiency of long-range corrected functionals for some properties of large compounds. J Chem Phys. 2007; 126:144105. [PubMed: 17444699]

46. Guthmuller J, Champagne B. Resonance Raman scattering of rhodamine 6G as calculated by time-dependent density functional theory: vibronic and solvent effects. J Phys Chem A. 2008; 112:3215–3223. [PubMed: 18327928]

47. Setiawan D, Kazaryan A, Martoprawiro MA, Filatov M. A first principles study of fluorescence quenching in rhodamine B dimers: How can quenching occur in dimeric species? Phys Chem Chem Phys. 2010; 12:11238–11244. [PubMed: 20676414]

48. Mütze J, et al. Excitation spectra and brightness optimization of two-photon excited probes. Biophys J. 2012; 102:934–944. [PubMed: 22385865]

49. Akerboom J, et al. Optimization of a GCaMP calcium indicator for neural activity imaging. J Neurosci. 2012; 32:13819–13840. [PubMed: 23035093]

50. Schindelin J, et al. Fiji: an open-source platform for biological-image analysis. Nat Methods. 2012; 9:676–682. [PubMed: 22743772]

51. Mosmann T. Rapid colorimetric assay for cellular growth and survival: application to proliferation and cytotoxicity assays. J Immunol Methods. 1983; 65:55–63. [PubMed: 6606682]

52. Kohl J, et al. Ultrafast tissue staining with chemical tags. Proc Natl Acad Sci U S A. 2014; 111:E3805–3814. [PubMed: 25157152]

53. Ji N, Milkie DE, Betzig E. Adaptive optics via pupil segmentation for high-resolution imaging in biological tissues. Nat Methods. 2010; 7:141–147. [PubMed: 20037592]

54. Sun W, Tan Z, Mensh BD, Ji N. Thalamus provides layer 4 of primary visual cortex with orientation- and direction-tuned inputs. Nat Neurosci. 2016; 19:308–315. [PubMed: 26691829]

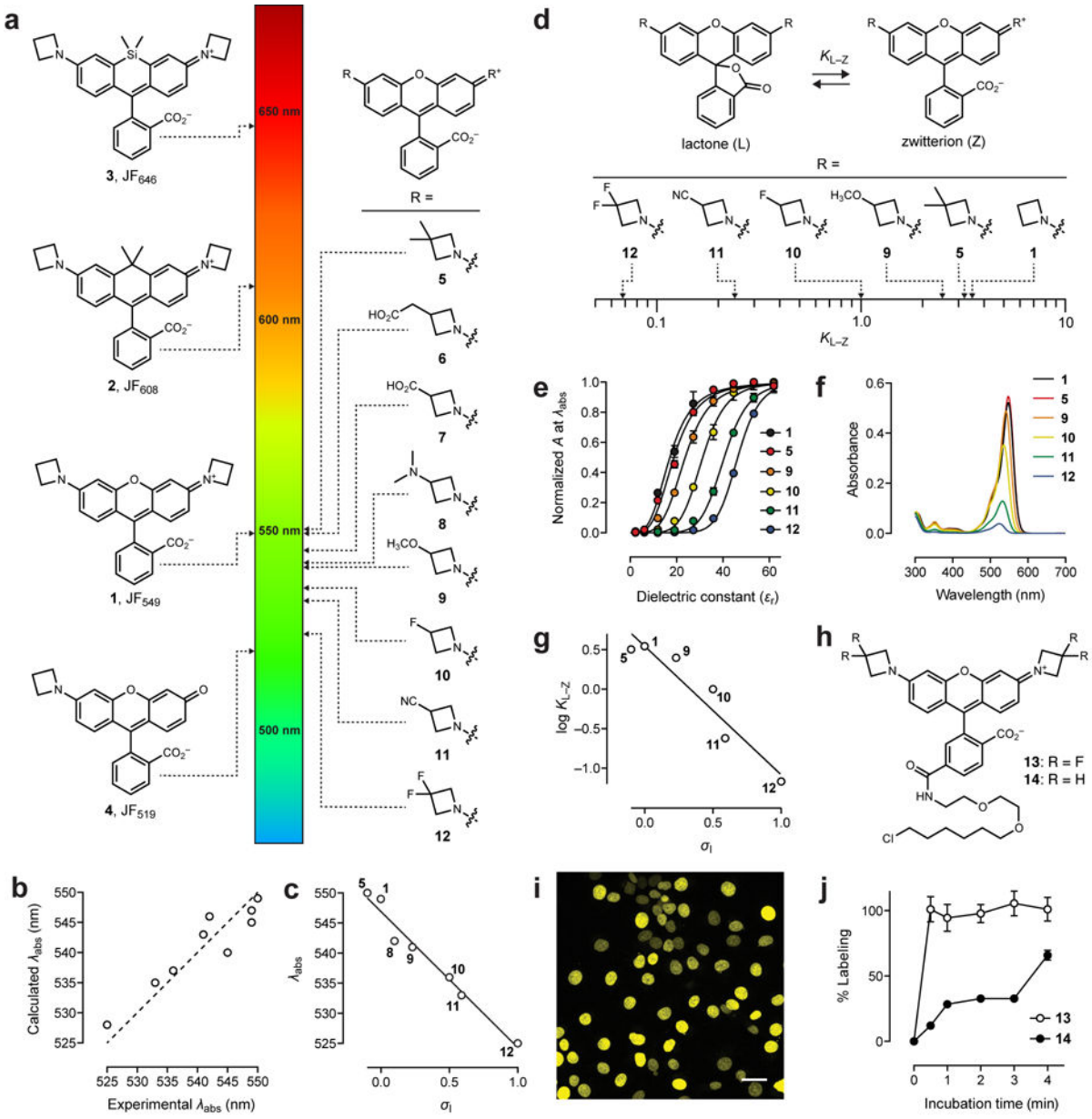

Figure 1. Fine-tuning rhodamine dyes

(**a**) Comparing coarse-tuning of λ_{abs} for dyes **1**–**4** and fine-tuning observed for azetidinyl rhodamines **5**–**12**. (**b**) Correlation between calculated (DFT) and experimental λ_{abs} values for dyes **1**, **5**–**12**; dashed line shows ideal fit. (**c**) Correlation of experimental λ_{abs} *vs.* inductive Hammett constants (σ_I) for dyes **1**, **5**, **8**–**12**. For the geminal disubstituted compounds **5** and **12** the σ_I of the substituent was doubled. Solid line shows linear regression ($R^2 = 0.97$). (**d**) Fine-tuning of the lactone–zwitterion equilibrium constant ($K_{L–Z}$) for dyes **1**, **5**, **9**–**12**. (**e**) Normalized absorption vs. dielectric constant (ε_r) for dyes **1**, **5**, and **9**–**12**; error bars show ± s.e.m; n = 4. (**f**) Absolute absorbance of **1**, **5**, **9**–**12** (5 μM) in 1:1 dioxane:H_2O. (**g**) Correlation of $K_{L–Z}$ *vs.* inductive Hammett constants (σ_I) for dyes **1**, **5**, **9**–**12**. For the geminal disubstituted compounds **5** and **12** the σ_I of the substituent was

doubled. Solid line shows linear regression ($R^2 = 0.91$). (**h**) Chemical structure of JF_{525}–HaloTag ligand **13** and JF_{549}–HaloTag ligand **14**. (**i**) Image of live, washed COS7 cells expressing histone H2B–HaloTag fusions and labeled with ligand **13**. Scale bar: 35 μm. (**j**) Plot of percent labeling of histone H2B–HaloTag fusions in live cells *vs.* incubation time for ligands **13** (100 nM) and **14** (100 nm); error bars show ± s.e.m; n = 113–248 (see Methods).

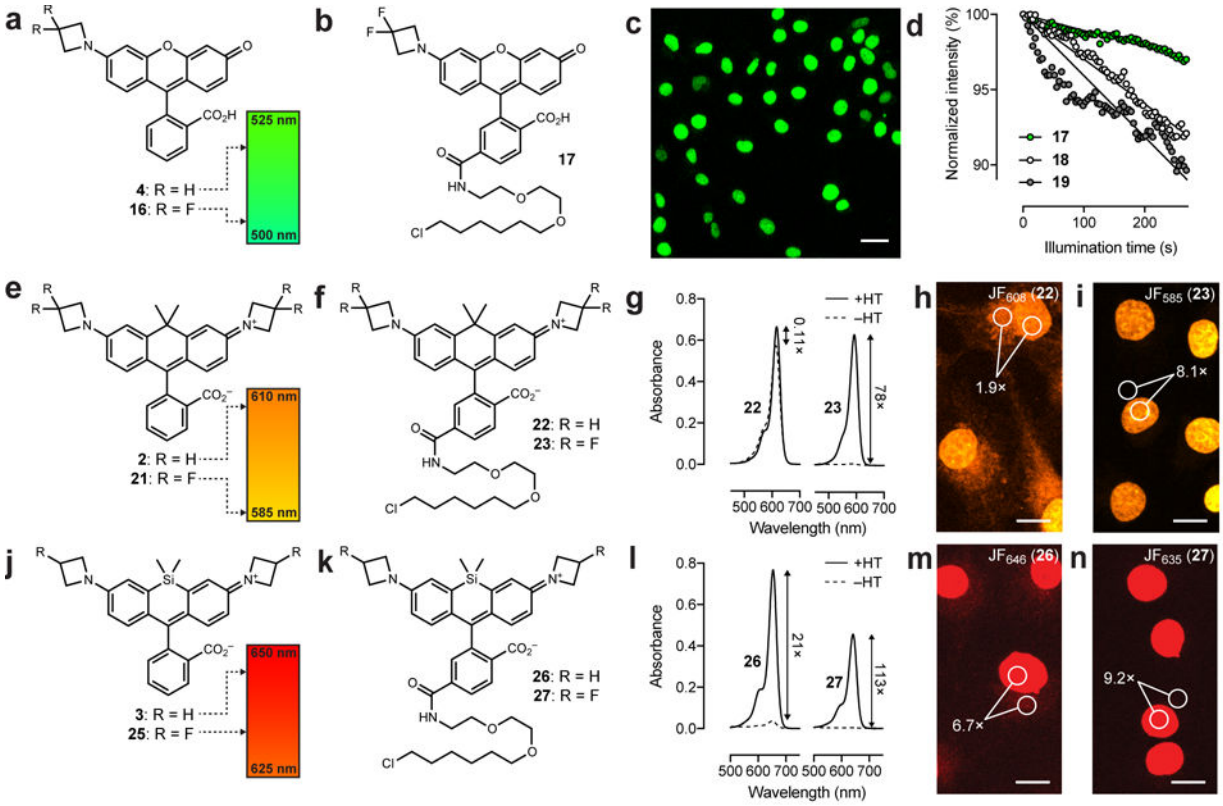

Figure 2. Rational fine-tuning of other dyes

(**a**) Tuning of JF_{519} (**4**) to yield JF_{503} (**16**). (**b**) Structure of JF_{503}–HaloTag ligand **17**. (**c**) Image of live, washed COS7 cells expressing histone H2B–HaloTag fusions and labeled with ligand **17**. Scale bar: 35 μm. (**d**) Comparison of the photostability of cells labeled with **17** and cells labeled with 488 nm-excited dyes **18** and **19** (Supplementary Fig. 2d); the initial photobleaching measurements are fitted to a linear regression. (**e**) Tuning of JF_{608} (**2**) to yield JF_{585} (**21**). (**f**) Structure of HaloTag ligands derived from JF_{608} (**22**) and JF_{585} (**23**). (**g**) Absorbance of HaloTag ligands **22** and **23** in the presence (+HT) or absence (–HT) of excess HaloTag protein; n = 2. (**h,i**) Representative images of COS7 cells expressing HaloTag–histone H2B fusion and labeled with 250 nM of HaloTag ligands **22** and **23** for 1 h and imaged directly without washing. The image for each dye pair was taken with identical microscope settings, λ_{ex} = 594 nm. Numbers indicate mean signal (nuclear) to background (cytosol) ratio (S/B) in three fields of view. (**h**) JF_{608} ligand **22** (S/B from n = 224 areas). (**i**) JF_{585} ligand **23** (S/B from n = 235 areas). (**j**) Tuning of JF_{646} (**3**) to yield JF_{635} (**25**). (**k**) Structure of HaloTag ligands derived from JF_{646} (**26**) and JF_{635} (**27**) (**l**) Absorbance of HaloTag ligands **26** and **27** in the presence (+HT) or absence (−HT) of excess HaloTag protein (n = 2). (**m,n**) Representative images of COS7 cells expressing HaloTag–histone H2B fusion and labeled with 250 nM of HaloTag ligands **26** and **27** for 1 h and imaged directly without washing. The image for each dye pair was taken with identical microscope settings, λ_{ex} = 647 nm. Numbers indicate mean signal (nuclear) to background (cytosol) ratio (S/B) in three fields of view. (**m**) JF_{646} ligand **26** (S/B from n = 175 areas). (**n**) JF_{635} ligand **27** (S/B from n = 278 areas). Scale bars for **h**,**i**,**m**,**n**: 15 μm.

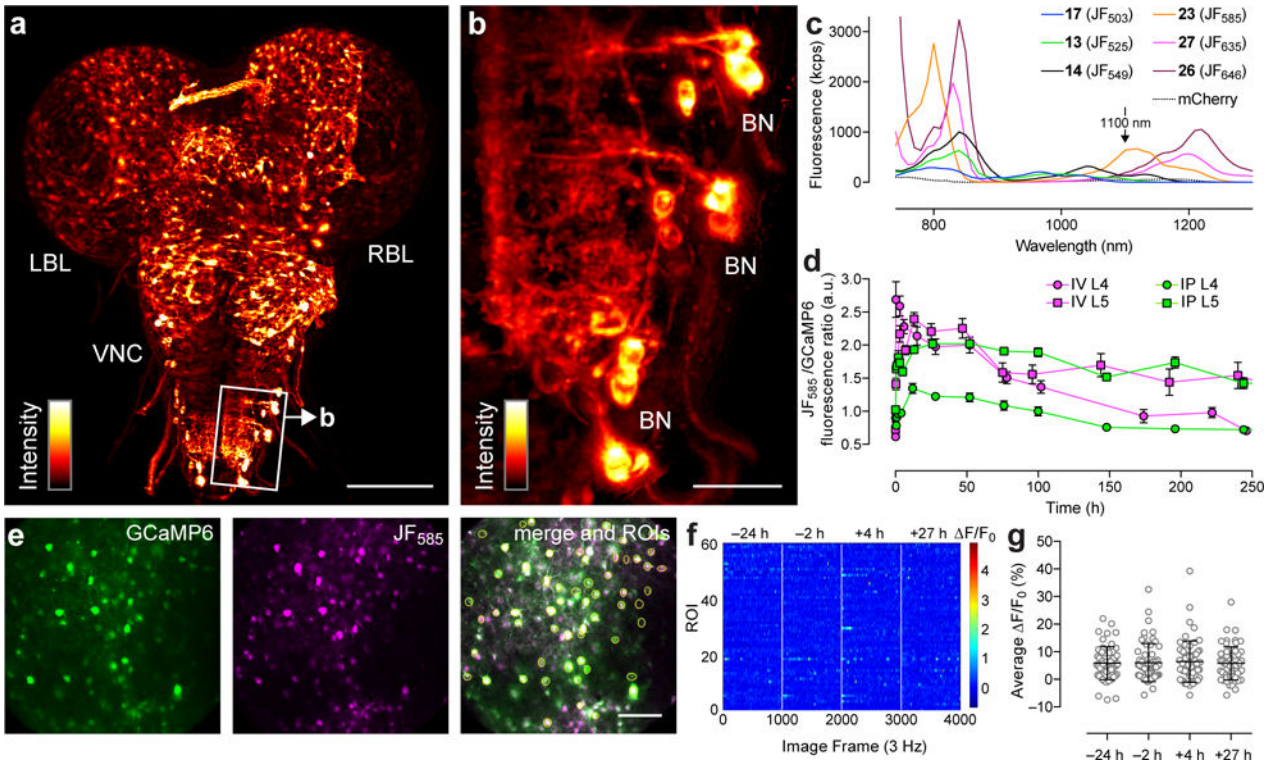

Figure 3. Labeling in tissue and *in vivo*

(**a**) SiMView light-sheet microscopy image (3D projection) of the central nervous system of a third instar *Drosophila* larva expressing myristoylated HaloTag protein in 'Basin' neurons (BNs) and stained with JF_{635}–HaloTag ligand (**27**); LBL: left brain lobe; VNC: ventral nerve cord; RBL: right brain lobe. Scale bar: 100 µm. (**b**) Zoom in of boxed area in panel **a** showing individual BN cell bodies. Scale bar: 20 µm. (**c**) Two-photon fluorescence excitation spectra of HaloTag conjugates (1 µM) from HaloTag ligands **13**, **14**, **17**, **23**, **26**, and **27** in 10 mM HEPES buffer (pH 7.3). The two-photon excitation spectra for mCherry is shown for reference. (**d**) Ratio of JF_{585} fluorescence to GCaMP6s epifluorescence at different time points after a single injection of JF_{585}–HaloTag ligand (**23**, 100 nmol) either intravenous (IV) or intraperitoneal (IP) into mice expressing HaloTag protein in either layer 4 (L4) or layer 5 (L5) cortical neurons; n = 3 fields of view; error bars show ± s.e.m. (**e**) Two-photon microscopy images of neurons in layer 5 of the visual cortex coexpressing GCaMP6s (green) and JF_{585}-labeled HaloTag (magenta) after IV injection of ligand **23** (t = 5 h). Scale bar: 100 µm. Yellow circles in the merged image indicate individual neurons as regions of interest (ROIs). (**f**) Raster plot of spontaneous neuronal activity in different ROIs (n = 61) before and after labeling with JF_{585}–HaloTag ligand (**23**). (**g**) Plot of average spontaneous neural activity in each ROI before and after labeling with JF_{585}–HaloTag ligand (**23**); central line shows mean; error bars show ± s.d.; no significant difference is observed between time points (one-way ANOVA: p = 0.95).

Table 1

Properties of azetidine-containing fluorophores **1**–**12, 16**, **21** and **25**.

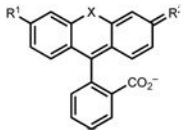

Dye	X	R^1	R^2	λ_{abs} (nm)	ε ($M^{-1}cm^{-1}$)	ε_{max} ($M^{-1}cm^{-1}$)[a]	λ_{em} (nm)	Φ	K_{L-Z}[b]
1 (JF_{549})				549	101,000	134,000	571	0.88	3.5
5				550	110,000	143,000	572	0.83	3.2
6		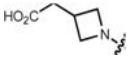	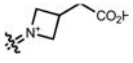	549	111,000	138,000	572	0.87	–
7		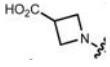	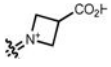	545	108,000	130,000	568	0.87	–
8		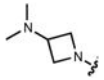	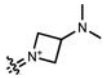	542	111,000	127,000	565	0.57[c]	–
9		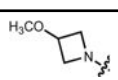	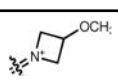	541	109,000	137,000	564	0.88	2.5
10				536	113,000	141,000	560	0.87	1.0
11		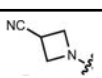	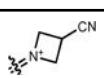	533	108,000	133,000	557	0.89	0.24
12 (JF_{525})		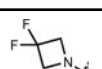	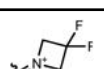	525	94,000	122,000	549	0.91	0.068

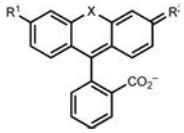

Dye	X	R[1]	R[2]	λ_{abs} (nm)	ε ($M^{-1}cm^{-1}$)	ε_{max} ($M^{-1}cm^{-1}$)[a]	λ_{em} (nm)	Φ	K_{L-Z}[b]
4 (JF_{519})				519	59,000	69,000	546	0.85	–
16 (JF_{503})				503	83,000	95,000	529	0.87	–
2 (JF_{608})				608	99,000	121,000	631	0.67	0.091
21 (JF_{585})				585	1,500	156,000	609	0.78	<0.0001
3 (JF_{646})				646	5,000	152,000	664	0.54	0.0012
25 (JF_{635})				635	~400	167,000	652	0.56	<0.0001

[a] maximal extinction coefficient measured in EtOH or TFE with 0.1%TFA (rhodamines) or 0.01% Et3N (rhodols)

[b] equilibrium constant measured in 1:1 v/v dioxane:water

[c] Φ = 0.89 in pH 5.0 buffer